

Cite this: *Chem. Sci.*, 2019, **10**, 3289 All publication charges for this article have been paid for by the Royal Society of Chemistry

Charge transfer dependence on CO₂ hydrogenation activity to methanol in Cu nanoparticles covered with metal–organic framework systems†

Hirokazu Kobayashi,^{*ab} Jared M. Taylor,^{‡a} Yuko Mitsuka,^c Naoki Ogiwara,^a Tomokazu Yamamoto,^{de} Takaaki Toriyama,^e Syo Matsumura^{def} and Hiroshi Kitagawa  ^{*afg}

We report the synthesis and characterization of highly active Cu nanoparticles covered with zirconium/hafnium-based metal–organic frameworks for CO₂ hydrogenation to methanol. Compared to Cu/γ-Al₂O₃, Cu/ZIF-8, Cu/MIL-100 and Cu/UiO-66 composites, UiO-66 acts as the most active support, with Cu/Zr-UiO-66 producing methanol at a rate 70 times higher than that of Cu/γ-Al₂O₃. In addition, the replacement of Zr⁴⁺ with Hf⁴⁺ in UiO-66 tripled in the rate of methanol production. Furthermore, we describe a substituent effect on the catalytic activity, with Cu/Zr-UiO66-COOH providing a three-fold enhancement of methanol production, compared to that of Zr-UiO-66 or Zr-UiO66-NH₂. The enhanced catalytic activity of Cu nanoparticles depends on the charge transfer degree from Cu nanoparticles to UiO-66 at the interface between Cu nanoparticles and UiO-66.

Received 5th December 2018
Accepted 30th January 2019DOI: 10.1039/c8sc05441j
rsc.li/chemical-science

Introduction

Hybrid materials composed of metal nanoparticles and metal–organic frameworks (MOFs) have attracted much attention for their gas storage, magnetic, optical and catalytic applications due to the remarkable synergistic function between their constituent materials.^{1–9} In particular, these hybrid materials have been investigated as highly selective and/or active catalysts because, based on MOF selection, surface properties such as pore size, hydrophobicity/hydrophilicity, and Lewis or Brønsted acidity/basicity can be tuned to control the functionality of the

composite.¹⁰ For example, Liyu Chen *et al.* reported Pd nanoparticles embedded in UiO-67 as a catalyst for selective olefin hydrogenation, with selectivity arising from molecular sieving by the pores of UiO-67.¹¹ Kyungsu Na *et al.* reported the hydrogenation of methylcyclopentane to produce selective products depending on the pore size of the Zr-based MOF support.⁵ So far, the strategies on the design for hybrid catalysts of metal nanoparticles and MOFs have been mainly based on the combination of their characteristics. On the other hand, hybrid catalysts with electronic interactions between metal and MOF have received scant attention.^{12–14} Since catalytic properties such as activity or selectivity strongly depend on the electronic states of the metal catalysts, tuning the electronic properties of metal nanoparticles by modifying a MOF support is of significance for further development of hybrid catalysts.

Carbon dioxide (CO₂) conversion into basic chemicals such as formic acid, methanol and carbon monoxide is very important not only for the reduction of CO₂ emissions, a greenhouse gas and major contributor to global warming, but also for the efficient use of CO₂ to achieve a carbon neutral energy cycle. In particular, methanol is a good energy carrier as it is a stable liquid under ambient conditions, and it can act as a starting material for the production of olefins, formalin and so on. For these reasons, the development of efficient catalysts for methanol synthesis by CO₂ hydrogenation has been extensively investigated, yet still remains a challenge as CO₂ is a stable gas molecule which requires a 6-electron reduction for conversion into methanol. So far, most research on CO₂ hydrogenation

^aDivision of Chemistry, Graduate School of Science, Kyoto University, Kitashirakawa-Oiwakecho, Sakyo-ku, Kyoto, 606-8502, Japan. E-mail: hkobayashi@kuchem.kyoto-u.ac.jp; kitagawa@kuchem.kyoto-u.ac.jp

^bJST, PRESTO, 4-1-8 Honcho, Kawaguchi, Saitama, 332-0012, Japan

^cShoei Chemical Inc., 5-3, Aza-wakazakura Fujinoki-machi, Tosu-shi, Saga 841-0048, Japan

^dDepartment of Applied Quantum Physics and Nuclear Engineering, Graduate School of Engineering, Kyushu University, Motoooka 744, Nishi-ku, Fukuoka, 819-0395, Japan

^eThe Ultramicroscopy Research Center, Kyushu University, Motoooka 744, Nishi-ku, Fukuoka, 819-0395, Japan

^fInamori Frontier Research Center, Kyushu University, 744 Motoooka, Nishi-ku, Fukuoka, 819-0395, Japan

[†]Institute for Integrated Cell-Material Sciences (iCeMS), Kyoto University, Yoshida, Sakyo-ku, Kyoto, 606-8501, Japan

† Electronic supplementary information (ESI) available. See DOI: 10.1039/c8sc05441j

‡ Present address: Department of Chemistry, University of Calgary, 2500 University Dr NW, Calgary, Alberta T2N 1N4 (Canada).



using MOF hybrid materials are related to CO (2-electron reduction) production,^{15,16} and there are few reports on CO₂ hydrogenation to methanol.^{7,13} Herein we describe highly active Cu nanoparticle composites for CO₂ hydrogenation to methanol, with activity controlled *via* charge transfer from Cu to UiO-66 by controlling the functional groups or metal species in the MOF for the first time.

For the MOF component of the composite material, we focused on Zr- and Hf-based UiO-66 (**Zr-UiO-66** and **Hf-UiO-66**, respectively), which consist of hexanuclear M⁴⁺ oxy/hydroxy clusters linked into a cubic 3-dimensional network by terephthalate linkers. These MOFs were chosen because they have superior thermal, water and chemical stabilities, and because they are easily functionalized through linker substitution or defect formation.^{17–19} For functionalization of the terephthalate, we selected carboxylate and amino groups. Carboxylate and amino groups are known to work as electron withdrawing and donating groups to benzene ring, respectively. Therefore, the electronic states of the Zr₆ cluster in UiO-66 are likely influenced by their substitution groups, which may lead to controlling the degree of charge transfer between Cu nanoparticles and UiO-66.

Results and discussion

Synthesis and characterization of Cu/UiO-66 composite catalysts

We synthesized **Cu/UiO-66** composite catalysts by thermal decomposition of copper acetylacetone, Cu(acac)₂ as a Cu precursor in the presence of the pre-synthesized MOF (see experimental details, ESI[†]). In a typical synthesis, **Zr-UiO-66** was firstly prepared by minor modifications to a solvothermal method reported previously.¹⁹ The obtained **Zr-UiO-66** and Cu(acac)₂ were then dispersed in an acetone solution, and the mixture was stirred at room temperature for 24 h. After impregnation, the solvent was removed by centrifugation. The collected solid, which included **Zr-UiO-66** and Cu(acac)₂, was heated at 350 °C for 1 h under vacuum to obtain the composite of **Zr-UiO-66** and Cu nanoparticles (**Cu/Zr-UiO-66**) (see experimental details, ESI[†]). **Cu/Hf-UiO-66**, **Cu/Zr-UiO-66-NH₂**, with a 2-aminoterephthalate linker, **Cu/Zr-UiO-66-COOH** with a 1,2,4-benzenetricarboxylate linker, and a γ -Al₂O₃ supported Cu catalyst (**Cu/ γ -Al₂O₃**) as a standard control catalyst were also prepared by the same method to compare their catalytic activity with the non-functionalized **Cu/Zr-UiO-66**.

The amounts of Cu loaded into **Cu/Zr-UiO-66**, **Cu/Zr-UiO-66-NH₂**, **Cu/Zr-UiO-66-COOH**, **Cu/Hf-UiO-66** and **Cu/ γ -Al₂O₃** were determined to be 14, 19, 19, 12 and 13 wt%, respectively, by inductively coupled plasma mass spectrometry. TEM images of the composites revealed that Cu nanoparticles are well dispersed and the mean diameters were estimated to be 13.1 \pm 3.9, 18.6 \pm 5.1, 19.6 \pm 4.0, 15 \pm 4.1 and 24 \pm 4.1 nm for **Cu/Zr-UiO-66**, **Cu/Zr-UiO-66-NH₂**, **Cu/Zr-UiO-66-COOH**, **Cu/Hf-UiO-66** and **Cu/ γ -Al₂O₃**, respectively (Fig. S1[†]).

Fig. 1a shows the powder X-ray diffraction (PXRD) patterns of **Cu/Zr-UiO-66**, **Cu/Zr-UiO-66-NH₂**, **Cu/Zr-UiO-66-COOH** and **Cu/Hf-UiO-66**. The PXRD patterns of all composite materials consist of the diffraction from both Cu and the corresponding

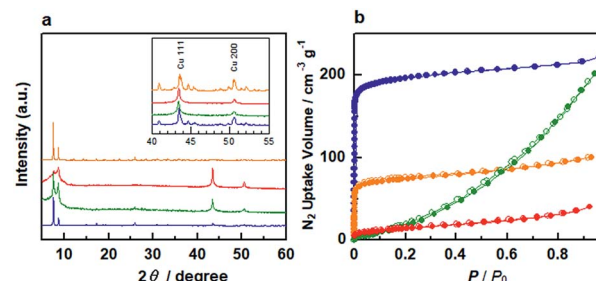


Fig. 1 (a) PXRD patterns and (b) N₂ adsorption/desorption isotherms at 77 K for Cu/Zr-UiO-66 (blue), Cu/Zr-UiO-66-NH₂ (green), Cu/Zr-UiO-66-COOH (red) and Cu/Hf-UiO-66 (orange).

UiO-66. **Cu/Zr-UiO-66-NH₂** and **Cu/Zr-UiO-66-COOH** showed weak diffraction peaks from the MOF component (Fig. S2[†]), which suggests a decrease in crystallinity, likely arising from some instability of these MOFs at the high temperatures needed to decompose Cu(acac)₂ (Fig. S3[†]).

In order to confirm the porosity of UiO-66 after hybridization with Cu nanoparticles, N₂ sorption isotherms of the composites were measured at 77 K (Fig. 1b). **Cu/Zr-UiO-66** and **Cu/Hf-UiO-66** show typical type-I sorption behavior originating from the microporosity of the MOF, with a decrease in total uptake *versus* the Cu free MOF due to the presence of Cu nanoparticles. In contrast, a sharp decrease in the microporosity is observed in **Cu/Zr-UiO-66-NH₂** and **Cu/Zr-UiO-66-COOH** corresponding to the lower crystallinity of these samples, which is consistent with the PXRD results. The calculated BET surface areas for **Cu/Zr-UiO-66**, **Cu/Hf-UiO-66**, **Cu/Zr-UiO-66-NH₂** and **Cu/Zr-UiO-66-COOH** were 702, 207, 172 and 52 m² g⁻¹, respectively, in comparison to 1368, 1427, 1074 and 201 m² g⁻¹ for the Cu free MOFs (Fig. S4[†]). From the extended X-ray absorption fine structure analysis, we confirmed that the local structures of Zr₆-clusters in **Cu/UiO-66** composite catalysts were maintained after hybridization with Cu nanoparticles (Fig. S5[†]).

In order to investigate the composite structure and elemental distribution in **Cu/Zr-UiO-66**, **Cu/Hf-UiO-66** and **Cu/Zr-UiO-66-COOH**, we performed high-angle annular dark-field scanning TEM (HAADF-STEM) and energy-dispersive X-ray (EDX) elemental mapping of Cu and the constituent elements of UiO-66 (Fig. 2). HAADF-STEM images and STEM-EDX mappings of **Cu/Zr-UiO-66**, **Cu/Zr-UiO-66-COOH** and **Cu/Hf-UiO-66** samples are shown in Fig. 2a–d, Fig. 2e–h and Fig. 2i–l, respectively. As shown in Fig. 2a, the HAADF-STEM image of **Cu/Zr-UiO-66** revealed that the MOF covers the Cu nanoparticles. Fig. 2b and c show the corresponding Cu-*K* and Zr-*L* maps which are the constituent metal elements of **Cu/Zr-UiO-66**, and Fig. 2d presents an overlay map of Cu and Zr. These mapping data clearly show that the Zr elements of UiO-66 are distributed around the surface of the Cu nanoparticles. Similarly, HAADF-STEM images and STEM-EDX mappings of **Cu/Zr-UiO-66-COOH** and **Cu/Hf-UiO-66** showed the same results as that of **Cu/Zr-UiO-66**. These results demonstrate that **Cu/Zr-UiO-66** and the analogues are hybrid structures where Cu nanoparticles are covered with UiO-66.

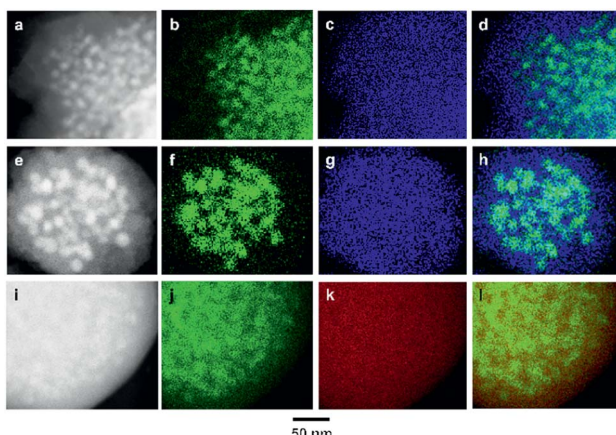


Fig. 2 (a) HAADF image, (b) Cu-*K* and (c) Zr-*L* STEM-EDX maps of Cu/Zr-UiO-66. (d) Reconstructed overlay image of the maps shown in panels (b) and (c) (green, Cu; blue, Zr). (e) HAADF image, (f) Cu-*K* and (g) Zr-*L* STEM-EDX maps of Cu/Zr-UiO-66-COOH. (h) Reconstructed overlay image of the maps shown in panels (f) and (g) (green, Cu; blue, Zr). (i) HAADF image, (j) Cu-*K* and (k) Hf-*L* STEM-EDX maps of Cu/Hf-UiO-66. (l) Reconstructed overlay image of the maps shown in panels (j) and (k) (green, Cu; red, Hf).

In order to address the possible formation mechanism on Cu nanoparticles covered with UiO-66, we performed the STEM-EDX mapping of the mixture of Zr-UiO-66 and Cu(acac)₂ after impregnation. The STEM-EDX mapping revealed that the Cu precursor was located inside the pores of Zr-UiO-66 (Fig. S6†). The N₂ sorption isotherm at 77 K indicated the decrease in the microporosity of Zr-UiO-66 due to incorporation of Cu(acac)₂ (Fig. S7†). The PXRD patterns of the mixture of Zr-UiO-66 and Cu(acac)₂ suggested that Cu(acac)₂ exists in an isolated state (Fig. S8†). Considering that the mean diameter of Cu nanoparticles (13.1 nm) in Cu/Zr-UiO-66 is larger than that of the pore size of UiO-66 (*ca.* 1 nm), Cu(acac)₂ loaded into the pores of Zr-UiO-66 is thermally decomposed to generate Cu atoms, and the Cu atoms migrate to form Cu nanoparticles by Ostwald ripening while partially eroding UiO-66. Consequently, Cu nanoparticles are preferentially present in the MOF particles.

CO₂ hydrogenation activity to methanol in Cu/UiO-66 composite catalysts

To investigate the catalytic activities of the Cu/UiO-66 composites for CO₂ hydrogenation to methanol, we performed the activity tests using a fixed bed flow reactor with a gas mixture of 20 sccm CO₂, 100 sccm H₂ and 20 sccm He, 2 atm at 220 °C (see experimental details, ESI†). The reaction temperature is lower than the thermally decomposed temperature of UiO-66 and the analogues (Fig. S3†). The amount of methanol synthesized by Cu/γ-Al₂O₃ and Cu/MOFs are shown in Fig. 3. The results of Cu composite catalysts with other well-known MOFs such as ZIF-8 and MIL-100 are also shown (Fig. S9 and 10†). It has been previously reported that Cu shows poor activity for the conversion of CO₂ into methanol.^{20,21} In our experiment, Cu/γ-Al₂O₃ also produced extremely small amounts of methanol (1.9 μmol g_{Cu}⁻¹ h⁻¹) (Fig. 3 inset). On the other hand, Cu/Zr-UiO-66

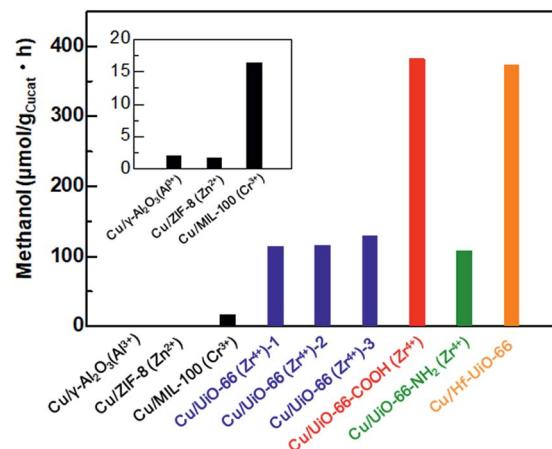


Fig. 3 The amount of methanol synthesized from CO₂ and H₂ using Cu/γ-Al₂O₃ and Cu/MOF composite catalysts. From elemental analysis and TGA, the amount of defects were estimated to be [Zr₆O₄(OH)₄(BDC)_{5,7}], [Zr₆O₄(OH)₄(BDC)_{4,5}(AcO)₃] and [Zr₆O₄(OH)₄(BDC)_{3,6}(AcO)_{4,8}] for Zr-UiO-66-1, Zr-UiO-66-2 and Zr-UiO-66-3, respectively. AcO = acetate.

exhibited a high catalytic activity, with a rate of methanol synthesis 70 times larger than that of Cu/γ-Al₂O₃ (114.2 μmol g_{Cu}⁻¹ h⁻¹). For comparison, pure Zr-UiO-66 does not show any catalytic activity for CO₂ hydrogenation. Taking into consideration that Cu/ZIF-8 and Cu/MIL-100 have poor CO₂ hydrogenation activities of 1.8 μmol g_{Cu}⁻¹ h⁻¹ and 16.4 μmol g_{Cu}⁻¹ h⁻¹, respectively (Fig. 3 inset), this result indicates that Zr-UiO-66 demonstrates a highly effective support effect for the Cu catalyst.

It has recently been reported that the defects in MOF play an important role for controlling properties such as gas sorption,²² proton conductivity,²³ optical properties^{24,25} and liquid phase catalytic activity.²⁶⁻²⁸ Furthermore, UiO-66 is well known to have widely controllable defect concentrations depending on the synthetic conditions.¹⁹ To investigate a defect effect on the catalytic activity of gas phase CO₂ hydrogenation, we synthesized Cu/Zr-UiO-66-1, Cu/Zr-UiO-66-2 and Cu/Zr-UiO-66-3 with increasing amounts of acetic acid to introduce increasing amounts of defects into the Zr₆-clusters (see experimental details and Fig. S11–S14†). Note: Cu/Zr-UiO-66 discussed above corresponds to Cu/Zr-UiO-66-2. As shown in Fig. 3, all of Cu/Zr-UiO-66-1, Cu/Zr-UiO-66-2 and Cu/Zr-UiO-66-3 exhibited high catalytic activities, compared to Cu/γ-Al₂O₃, but provided similar rates of methanol synthesis (114.2, 115.5 and 128.0 μmol g_{Cu}⁻¹ h⁻¹ for Cu/Zr-UiO-66-1, Cu/Zr-UiO-66-2 and Cu/Zr-UiO-66-3, respectively). These results indicate that the reactivity of CO₂ is not strongly affected by the defects in Zr₆-clusters of UiO-66. In addition, the N₂ sorption isotherms of Cu/Zr-UiO-66-1, Cu/Zr-UiO-66-2 and Cu/Zr-UiO-66-3 (Fig. S14†) indicated that the porosity of UiO-66 also does not directly affect the catalytic activity.

Ligand substitution in Cu/Zr-UiO-66 seemed to have a major effect on the rate of methanol synthesis with a nearly 3-fold enhancement using carboxylate functionalized Cu/Zr-UiO-66-COOH (381.5 μmol g_{Cu}⁻¹ h⁻¹ vs. 114.2 μmol g_{Cu}⁻¹ h⁻¹), but little



effect with the amine functionalized **Cu/Zr-UiO-66-NH₂** (107.7 $\mu\text{mol g}_{\text{Cu}}^{-1} \text{h}^{-1}$). Metal substitution for Hf in **Cu/Hf-UiO-66** also caused a nearly 3-fold enhancement compared to **Cu/Zr-UiO-66** (373.2 $\mu\text{mol g}_{\text{Cu}}^{-1} \text{h}^{-1}$ vs. 114.2 $\mu\text{mol g}_{\text{Cu}}^{-1} \text{h}^{-1}$). The catalytic activities of **Cu/UiO-66-COOH** and **Cu/Hf-UiO-66** were higher than that of the commercially used **Cu/ZnO/γ-Al₂O₃** system.²⁹ In addition, all of the catalysts (**Cu/Zr-UiO-66**, **Cu/Zr-UiO-66-NH₂**, **Cu/Zr-UiO-66-COOH** and **Cu/Hf-UiO-66**) gave very high selectivity of over 95% for methanol (Fig. S15†), which is in good agreement with the reported results.¹³

In general, the catalytic activity tends to increase with increasing BET surface area of the catalysts because the reactants can more easily access the surface of catalysts. The BET surface areas of **Cu/Hf-UiO-66** and **Cu/Zr-UiO-66-COOH** in this report were much smaller than that of **Cu/Zr-UiO-66**, although they exhibited significantly enhanced catalytic activities. In addition, the mean diameters of Cu nanoparticles in **Cu/Hf-UiO-66** and **Cu/Zr-UiO-66-COOH** are slightly larger than that of **Cu/Zr-UiO-66**. These results demonstrate that the surface area of UiO-66 does not directly affect the CO₂ hydrogenation activity, but rather the functional group or metal species is a significant factor. In addition, considering that Cu nanoparticles deposited on UiO-66 produced a smaller amount of methanol (67.8 $\mu\text{mol g}_{\text{Cu}}^{-1} \text{h}^{-1}$) (Fig. S16†), compared with that of **Cu/Zr-UiO-66-2**, the interface between Cu and UiO-66 is also critical to the enhanced catalytic activity.

It has been reported that charge transfer between metal nanoparticles and MOF plays an important role in altering the surface/bulk properties of nanoparticles.^{1,12–14} To investigate possible charge transfer between Cu and MOF, we performed X-ray photoelectron spectroscopy (XPS) of the MOF before and after the hybridization with Cu nanoparticles. As shown in Fig. 4a and b, for **Cu/UiO-66** and **Cu/UiO-66-COOH**, the Zr 3d binding energies shifted to lower binding energy after hybridization with Cu nanoparticles, which indicates that Zr⁴⁺ is in a partially reduced state. In contrast, the Cu 2p binding energies of **Cu/UiO-66** and **Cu/UiO-66-COOH** shifted to higher energies

with UiO-66 coating, although the shifts became obscured due to the surface oxidation of Cu upon exposure to air (Fig. S17†). These results suggest that charge transfer from Cu nanoparticles to **UiO-66** or **Cu/UiO-66-COOH** occurs in the composites. On the other hand, in the cases of **Cu/γ-Al₂O₃** and **Cu/ZIF-8** (Fig. 4c and d), the binding energy shifts of Al 2p and Zn 2p were not observable before and after the hybridization with Cu nanoparticles. The relationship between the produced methanol and the binding energy shift estimated by XPS analysis for **Cu/γ-Al₂O₃** and **Cu/MOF** catalysts is shown in Fig. 5 (Fig. S18 and Table S1†). As shown in Fig. 5, we can clearly see a correlation between the charge transfer and the amount of the produced methanol – the negative shift of the MOF contributes to the catalytic activity for CO₂ hydrogenation to methanol. In particular, among **Zr-UiO-66** and the analogues such as **Zr-UiO66-NH₂** and **Zr-UiO66-COOH**, the largest negative shift is observed in **Zr-UiO66-COOH**, which provided the largest rate of methanol synthesis (314.3 $\mu\text{mol g}_{\text{Cu}}^{-1} \text{h}^{-1}$). These results are the first demonstration of altering the catalytic activity of Cu nanoparticles *via* charge transfer from Cu to UiO-66 by controlling the functional group or metal species in the MOF. **Hf-UiO-66** showed a smaller binding energy shift (−0.17 eV), compared to **Zr-UiO66-COOH** (−0.32 eV) although the **Cu/Hf-UiO-66** composite demonstrates a catalytic activity comparable with the most active **Cu/UiO-66-COOH**. This is because the binding energy shift of Hf 4f is considered to be relatively smaller than that of Zr 3d due to the valence change.³⁰

The PXRD and TEM measurements revealed that the pristine structures of the **Cu/UiO-66** catalysts were maintained after the CO₂ hydrogenation test (Fig. S19 and S20†). Furthermore, after 5 cycles, the catalytic performance of **Cu/Zr-UiO66-COOH** had no obvious change (Fig. S21†), indicating stability of **Cu/Zr-UiO66-COOH** with excellent catalytic performance.

From theoretical calculations,³¹ the rate-determining step for CO₂ conversion into methanol is hydrogenation of formate, so the stabilization of formate is key to produce methanol at a high

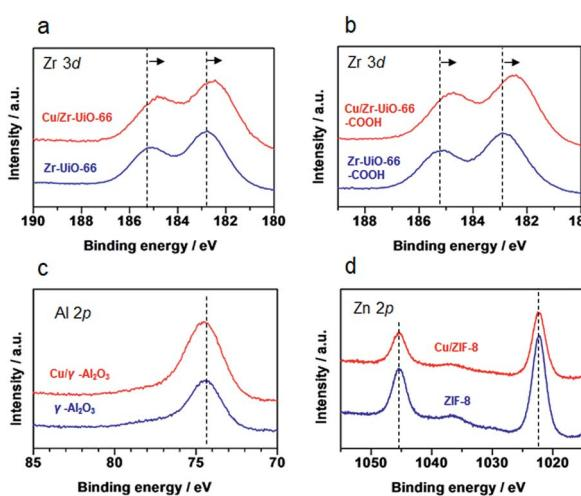


Fig. 4 XPS spectra of γ -Al₂O₃ and MOF before and after the hybridization with Cu nanoparticles. (a) **Cu/Zr-UiO-66**, (b) **Zr-UiO-66-COOH**, (c) γ -Al₂O₃ and (d) **ZIF-8**.

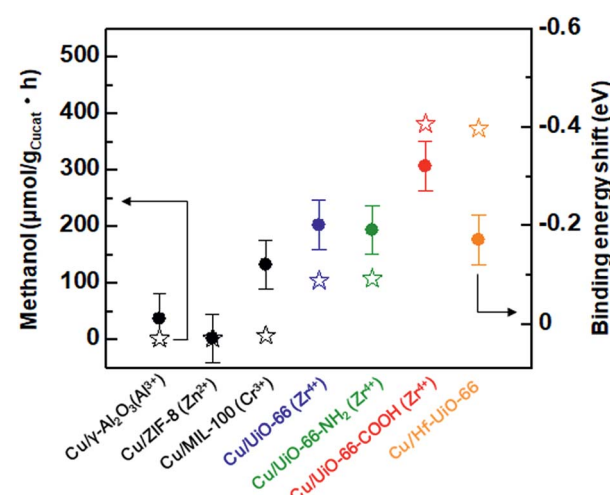


Fig. 5 Relationship between the synthesized methanol and binding energy shift estimated by XPS analysis for **Cu/γ-Al₂O₃** and **Cu/MOF** catalysts. Star and circle correspond to synthesized methanol and binding energy shift, respectively.



rate. It is also known that cationic Cu species helps to stabilize the intermediates (formate).³² Therefore, in our system, cationic Cu species due to charge transfer from Cu to the metal components of UiO-66 is considered to promote the stabilization of formate, leading to the enhancement of catalytic activity for CO₂ conversion into methanol.

Conclusions

In summary, we first demonstrated the charge transfer dependence on CO₂ hydrogenation activity to methanol in Cu/ MOF systems. Compared to Cu/γ-Al₂O₃, Cu/ZIF-8, Cu/MIL-100 and Cu/UiO-66 composites, UiO-66 is demonstrated to have the most highly effective support effect for CO₂ hydrogenation to methanol, and Cu/Zr-UiO-66 produced methanol at a rate 70 times larger than that of Cu/γ-Al₂O₃. The activity of CO₂ hydrogenation to methanol did not strongly correlate to the amount of defects in the Zr₆-clusters of UiO-66. On the other hand, the replacement of Zr⁴⁺ with Hf⁴⁺ in UiO-66 tripled the rate of methanol production. Furthermore, we found a substituent effect to the catalytic activity, with Cu/Zr-UiO66-COOH providing a 3-fold increase in the rate of methanol produced compared to that of Zr-UiO-66 or Zr-UiO66-NH₂. The charge transfer from Cu to UiO-66 is considered to play an important role in these enhancements of the catalytic activity of Cu. We hope that the results in this study will contribute to the further development of effective catalysts for CO₂ hydrogenation to methanol, as well as to the future design of highly novel catalysts based on control of the charge transfer between metal nanoparticles and MOF by careful selection of the functional group and/or metal species.

Conflicts of interest

There are no conflicts to declare.

Acknowledgements

This work was supported by NEDO, JST PRESTO (No. JPMJPR1514) and a Grant-in-Aid for Scientific Researches (B) (No. 17750056) from JSPS. The synchrotron radiation experiments were performed at the BL14B2 of SPring-8 with the approval of JASRI (Proposal No. 2018A1753). The STEM observations were performed as part of a program conducted by the Advanced Characterization Nanotechnology Platform sponsored by the MEXT, Japan.

Notes and references

- 1 G. Li, H. Kobayashi, J. M. Taylor, R. Ikeda, Y. Kubota, K. Kato, M. Takata, T. Yamamoto, S. Toh, S. Matsumura and H. Kitagawa, *Nat. Mater.*, 2014, **13**, 802–806.
- 2 C. M. Doherty, E. Knystautas, D. Buso, L. Villanova, K. Konstas, A. J. Hill, M. Takahashi and P. J. Falcaro, *Mater. Chem.*, 2012, **22**, 11470–11474.
- 3 P. Falcaro, F. Normandin, M. Takahashi, P. Scopece, H. Amenitsch, S. Costacurta, C. M. Doherty, J. S. Laird,

- 4 M. D. H. Lay, F. Lisi, A. J. Hill and D. Buso, *Adv. Mater.*, 2011, **23**, 3901–3906.
- 5 Y. Zhao, N. Kornienko, Z. Liu, C. Zhu, S. Asahina, T. R. Kuo, W. Bao, C. Xie, A. Hexemer, O. Terasaki, P. Yang and O. M. Yaghi, *J. Am. Chem. Soc.*, 2015, **137**, 2199–2202.
- 6 K. Na, K. M. Choi, O. M. Yaghi and G. A. Somorjai, *Nano Lett.*, 2014, **14**, 5979–5983.
- 7 B. An, J. Zhang, K. Cheng, P. Ji, C. Wang and W. Lin, *J. Am. Chem. Soc.*, 2017, **139**, 3834–3840.
- 8 M. Zhao, K. Deng, L. He, Y. Liu, G. Li, H. Zhao and Z. Tang, *J. Am. Chem. Soc.*, 2014, **136**, 1738–1741.
- 9 G. Li, S. Zhao, Y. Zhang and Z. Tang, *Adv. Mater.*, 2018, **30**, 1800702.
- 10 Q. Yang, Q. Xu and H.-L. Jiang, *Chem. Soc. Rev.*, 2017, **46**, 4774–4808.
- 11 L. Chen, H. Chen, R. Luque and Y. Li, *Chem. Sci.*, 2014, **5**, 3708–3714.
- 12 M. Zhao, K. Yuan, Y. Wang, G. Li, J. Guo, L. Gu, W. Hu, H. Zhao and Z. Tang, *Nature*, 2016, **539**, 76–80.
- 13 B. Rungtaweevoranit, J. Baek, J. R. Araujo, B. S. Archanjo, K. M. Choi, O. M. Yaghi and G. A. Somorjai, *Nano Lett.*, 2016, **16**, 7645–7649.
- 14 S. Yoshimasu, M. Sadakiyo, A. Staykov, K. Kato and M. Yamauchi, *Chem. Commun.*, 2017, **53**, 6720–6723.
- 15 K. M. Choi, D. Kim, B. Rungtaweevoranit, C. A. Trickett, J. T. D. Barmanbek, A. S. Alshammari, P. Yang and O. M. Yaghi, *J. Am. Chem. Soc.*, 2017, **139**, 356–362.
- 16 X. Zhao, H. Xu, X. Wang, Z. Zheng, Z. Xu and J. Ge, *ACS Appl. Mater. Interfaces*, 2018, **10**, 15096–15103.
- 17 J. H. Cavka, S. Jakobsen, U. Olsbye, N. Guillou, C. Lamberti, S. Bordiga and K. P. Lillerud, *J. Am. Chem. Soc.*, 2008, **130**, 13850–13851.
- 18 S. Biswas and P. V. D. Voort, *Eur. J. Inorg. Chem.*, 2013, **12**, 2154–2160.
- 19 H. Wu, Y. S. Chua, V. Krungleviciute, M. Tyagi, P. Chen, T. Yildirim and W. Zhou, *J. Am. Chem. Soc.*, 2013, **135**, 10525–10532.
- 20 Y. Yang, J. Evans, J. A. Rodriguez, M. G. White and P. Liu, *Phys. Chem. Chem. Phys.*, 2010, **12**, 9909–9917.
- 21 Y. Yang, M. G. White and P. Liu, *J. Phys. Chem. C*, 2012, **116**, 248–256.
- 22 O. Kozachuk, I. Luz, F. X. L. Xamena, H. Noei, M. Kauer, H. B. Albada, E. D. Bloch, B. Marler, Y. Wang, M. Muhler and R. A. Fischer, *Angew. Chem., Int. Ed.*, 2014, **53**, 7058–7062.
- 23 J. Taylor, S. Dekura, R. Ikeda and H. Kitagawa, *Chem. Mater.*, 2015, **27**, 2286–2289.
- 24 Z. Fang, J. P. Dirholt, M. Kauer, W. Zhang, C. Lochenie, B. Jee, B. Albada, N. Metzler-Nolte, A. Pcppl, B. Weber, M. Muhler, Y. Wang, R. Schmid and R. A. Fischer, *J. Am. Chem. Soc.*, 2014, **136**, 9627–9636.
- 25 C. L. Whittington, L. Wojtas and R. W. Larsen, *Inorg. Chem.*, 2014, **53**, 160–166.



26 C. Chizallet, S. Lazare, D. B.-Bachi, F. Bonnier, V. Lecocq, E. Soyer, A.-A. Quoineaud and N. Bats, *J. Am. Chem. Soc.*, 2010, **132**, 12365–12377.

27 L. T. L. Nguyen, K. K. A. Le, H. X. Truong and N. T. S. Phan, *Catal. Sci. Technol.*, 2012, **2**, 521–528.

28 K. Leus, I. Muylaert, M. Vandichel, G. B. Marin, M. Waroquier, V. V. Speybroeck and P. V. D. Voort, *Chem. Commun.*, 2010, **46**, 5085–5087.

29 Manuscript in preparation.

30 *X-ray Photoelectron Spectroscopy Database*, <http://techdb.podzone.net/eindex.html>.

31 Y. Yang, C. A. Mims, D. H. Mei, C. Peden and C. T. Campbell, *J. Catal.*, 2013, **298**, 10–17.

32 C. Liu, B. Yang, E. Tyo, S. Seifert, J. DeBartolo, B. v. Issendorff, P. Zapol, S. Vajda and L. A. Curtiss, *J. Am. Chem. Soc.*, 2015, **137**, 8676.

